Dynamical Evolution of Earth Mini-Moon 2020 CD$_3$: Role of Invariant Manifold

B. Dermawan[1], I. Nurul Huda[2,3], M. D. Danarianto[3], M. B. Saputra[4,3], H. S. Ramadhan[4]

[1] Department of Astronomy and Bosscha Observatory, Institut Teknologi Bandung, Bandung, Indonesia.

[2] School of Astronomy and Space Science, Key Laboratory of Modern Astronomy and Astrophysics (Ministry of Education), Nanjing University, Nanjing 210023, PR China.

[3] Research Center for Computing, National Research and Innovation Agency, Bogor, Indonesia.

[4] Departemen Fisika, FMIPA, Universitas Indonesia, Depok, Indonesia

`budider@itb.ac.id`

Abstract. Asteroid 2020 CD$_3$ is one of the Earth's Temporary Captured Orbiters. This study aims to investigate the dynamical evolution of the asteroid, notably its pre-capture and post-capture phases. The dynamics was analyzed through the framework of Circular Restricted Three-Body Problem with the Sun and the Earth-Moon system as primaries. We investigated the role of invariant manifold from Lyapunov and Halo orbits to the asteroid motion. It shows that the invariant manifold of Lyapunov orbit may play a significant role for guiding the asteroid to enter the Hill region of Earth through the Lagrange point L_1. We also discovered that the invariant manifold of Lyapunov orbit guides the asteroid after the escape process from L_2. In contrast, we found that the asteroid differs from Halo orbit's invariant manifold, both for pre- and post-captured periods.

Key words: CRTBP, Invariant Manifold, 2020 CD$_3$

Introduction

The Temporally Captured Orbiter (TCO) is an object that is gravitationaly locked by a planet and becomes its temporal natural satellite. There are two criteria for classifying an object as a TCO. First, its planetocentric energy must be negative, and second, it must complete at least one orbit around the planet [Rickman & Malmort(1981)]. Several asteroids have been found to behave as the Earth's TCOs. The first discovered asteroid to experience a temporary capture by the Earth is the 1991 VG [Tancredi(1997)]. This object orbited the Earth for about a month in February 1992. Several years later, the asteroid 2006 RH$_{120}$ was also discovered to be captured by the Earth. Unlike the 1991 VG, this asteroid orbited the Earth much longer, from July 2006 to July 2007 [Kwiatkowski et al.(2009)]. Another known temporal satellite of the Earth is the asteroid 2020 CD$_3$. It was observed in mid-February 2020 and did continue orbiting the Earth until mid-May 2020. A numerical study suggests that the asteroid was captured by the Earth between 2011 and 2018. It escaped in 2020 and may be captured again in the future [de la Fuente Marcos & de la Fuente Marcos(2020)]. Recently, objects have been found that became known as Earth 'mini-moons', such as 2022 NX$_1$ and 2024 PT$_5$ [de la Fuente Marcos et al.(2023), de la Fuente Marcos & de la Fuente Marcos(2024), see e.g.]. However, these objects are not TCOs since they do not complete a full orbit around the Earth.

Although only three minor bodies have been confirmed as Earth's TCOs, and other objects merely fly by Earth, there remains a possibility that Earth hosts several mini-satellites [Granvik et al.(2012)]. Moreover, Fedorets et al.

[Fedorets et al.(2020)] predicted that the upcoming Large Synoptic Survey Telescope could detect a TCO once every year or even every two months. There are at least two advantages in studying the TCOs. First, it provides a scientific benefit, as understanding this phenomenon can contribute to the development of theories regarding the origin of natural satellites [Heppenheimer(1975), Horedt(1976)]. Second, the TCOs become potential objects for capture and mining [Anderson & Lo(2018)]. Hence, understanding the behaviour of these objects' motion is important for the future of satellite missions.

The dynamics of minor bodies can be investigated through the framework of Circular Restricted Three-Body Problem (CRTBP). This concept is particularly implementable to minor bodies that experience capture event by a planet, as they are predominantly bounded by two primary objects, i.e. the Sun and the planet, and have negligible mass compared to the primary bodies. In recent developments, several authors have used this approach by focusing on the role of invariant manifold in the dynamics of minor bodies. [Howell et al.(2001)] used this approach to study the orbital evolution of comets Helin–Roman–Crockett and Oterma, which experienced a capture event with Jupiter. They concluded that the orbits of these comets are well described by the invariant manifold of the periodic orbit equilibrium point. This statement was reinforced by [Koon et al.(2001)] who suggested that the invariant manifold structures of L_1 and L_2 have facilitated the temporary capture of some short-period comets by Jupiter. More recently, [Swenson et al.(2019)] used the three-body approach to understand the capture of comet Shoemaker-Levy 9 by Jupiter. They concluded that the orbit of this comet partly follows the invariant manifold of Sun-Jupiter system. For the case of Earth's TCOs, [Anderson & Lo(2016)] studied the dynamical evolution of the asteroid 2006 RH_{120} under the framework of CRTBP. They used the invariant manifold theory and focused on the orbital evolution before and after the capture event. This work was extended by [Anderson & Lo(2018)] to study the dynamical evolution during the capture event itself. Unlike the previous study, they treated the trajectory in the Elliptic Restricted Three-Body Problem.

In this study, we aim to investigate the pre- and post-capture phases of the asteroid 2020 CD_3. We analyze the asteroid trajectory in the framework of the CRTBP. The rest of this paper is structured as follows: Section 1 provides a detailed explanation about the data and method used. Section 2 describes the analysis of the asteroid's motion within the CRTBP framework. Finally, the conclusion of this study is given in the last Section.

1   Data and Method

In the CRTBP analysis, we simplify the system as follows. First, we consider that the Earth has a circular orbit. Second, we treat the Earth and the Moon as a single mass located at the Earth-Moon barycenter, hereafter referred to as "Earth-Moon". Third, we consider the primaries as point mass objects. Let m_1 and m_2 be the masses of Sun and the Earth-Moon, respectively. Here, the asteroid 2020 CD_3 is called the "third body". In the case of the three-body problem, it is more convenient to introduce the system in rotational coordinates (X, Y, Z). The primaries are located in the X-axis with the distance
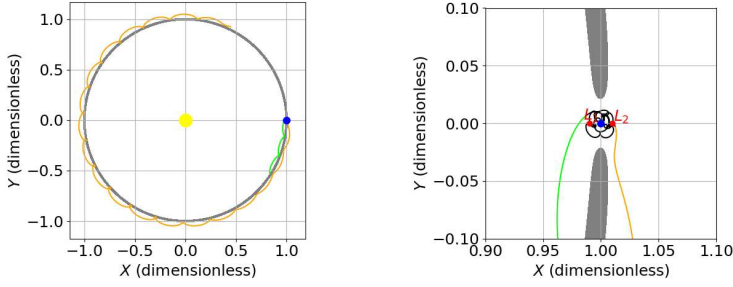
Fig. 2: The orbital evolution of 2020 CD$_3$ during pre-capture (green), post-capture (orange), and capture event (black) phases in the time interval between 2015 - 2050. Here, panel (b) is a zoomed-in version of panel (a). The Sun and Earth-Moon barycenter are represented as yellow and blue dots, respectively. Grey color represents the forbidden region.

between primaries chosen as the unit of length. The time unit is chosen by setting the angular momentum of the system to one. The equations of motion of the third object in the CRTBP are given as follows

$$\ddot{X} - 2\dot{Y} = \frac{\partial U}{\partial X},$$
$$\ddot{Y} + 2\dot{X} = \frac{\partial U}{\partial Y}, \tag{1}$$
$$\ddot{Z} = \frac{\partial U}{\partial Z},$$

where U is a pseudo-potential function of

$$U = \frac{1}{2}\left(X^2 + Y^2\right) + \frac{(1-\mu)}{r_1} + \frac{\mu}{r_2}, \tag{2}$$

with

$$r_1^2 = (X + \mu)^2 + Y^2 + Z^2,$$
$$r_2^2 = (X - (1-\mu))^2 + Y^2 + Z^2. \tag{3}$$

Here, $\mu = m_2/(m_1 + m_2)$ is called the mass parameter. We took the values of the Sun, Earth, and Moon masses from [Park et al.(2021)]. These equations of motion are used in this study to generate the trajectory of the asteroid in the restricted three-body framework. Here, we used the circular approximation to the orbit since the ellipticity of the planet has small effect on this problem [Heppenheimer(1975)]. The integral of motion can be written by

$$\dot{X}^2 + \dot{Y}^2 + \dot{Z}^2 = 2U - C, \tag{4}$$

where C is called Jacobi constant or Jacobi integral. The Jacobi constant has a fixed value in the ideal CRTBP. This parameter plays an important role in

dynamical analysis since it determines the allowable trajectory of the third body.

The CRTBP has five equilibrium points, $L_{1,2,3,4,5}$. Three of these points are called collinear points (L_1, L_2, L_3) since they are located on the X-axis while the other two are called triangular points (L_4, L_5) as they form equilateral triangles with the two massive bodies. Here, we focus on L_1 and L_2 since they serve as a gateways for the third body to enter the Hill region.

Previous studies have identified the existence of an infinite number of periodic orbits in the region near collinear Lagrange points [Szebehely(1967)]. Each periodic orbit exists at a different energy level or has a unique Jacobi constant. Therefore, in order to study the dynamics of a small body which passes the periodic orbit, one has to be consider the same Jacobi constant with the corresponding small body. Here we consider two types of periodic orbit located in near L_1 and L_2: Lyapunov and Halo orbits. According to [Richardson(1980)], the linearized solution of the Halo orbit is

$$
\begin{aligned}
X &= -B_X \cos \omega t + \alpha \\
Y &= k B_X \cos \omega t + \alpha \\
Z &= B_Z \cos \omega t + \beta,
\end{aligned}
\tag{5}
$$

where B_X and B_Z are the amplitude of halo periodic orbit in the X and Z directions, respectively, ω is the frequency, while α and β are the phases of the in-plane and out-of-plane motions, respectively. Meanwhile, we only consider the first two equations of Eq. (5) for the linearized solution of the Lyapunov orbit. The initial values of the orbital periods are computed using the analytical method of [Richardson(1980)]. A correction to the initial condition has to be done to find the real periodic orbit. Here we used the shooting method to correct these initial conditions as given by [Parker & Anderson(2014)].
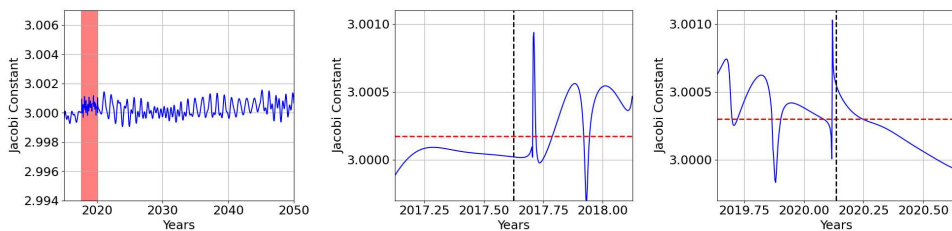

Fig. 4: The Jacobi constant during the orbital evolution of 2020 CD$_3$. (a) Jacobi constant from 2015 to 2050. (b) Jacobi constant 0.5 years before and after t_{pre}. (c) Jacobi constant 0.5 years before and after t_{post}. The red zone in (a) signifies the approximate time of the capture event. Dashed red and black lines in (b) represent the mean value of Jacobi constant and the time of capture event respectively. The dashed red and black lines in (c) are similar to (b), except they are for the escape event.

Lyapunov and Halo periodic orbits are unstable. Therefore, there exist a number of asymptotic trajectories that either approach or depart from a
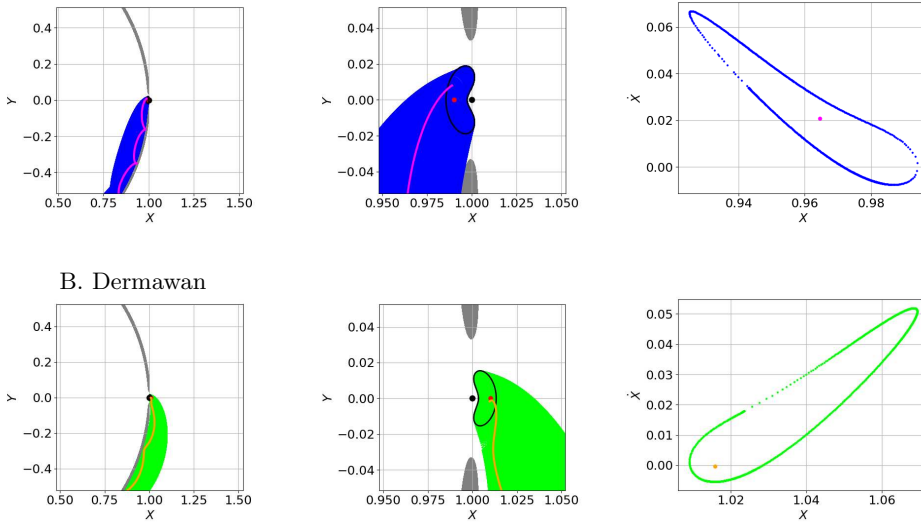
B. Dermawan

Fig. 6: The orbital evolution of 2020 CD₃ (a,b,d and e) and its Poincaré sections (c and f). Pre- and post-capture orbits are shown in magenta and orange, respectively. The black line represents the Lyapunov orbit, and grey zone signifies the forbidden region. The blue and green lines indicate the stable and unstable invariant manifolds, respectively. Earth is symbolized by a black dot, while the equilibrium points are represented by red dots. Here, (b) and (e) are the zoomed-in version of (a) and (d), respectively. The Poincaré surfaces of sections are shown in (c) and (f) for stable and unstable invariant manifolds, respectively. We cut the trajectory at $Y = -0.05$ to estimate the Poincaré sections

periodic orbit. These tube-like trajectories are known as invariant manifold. There are two kinds of invariant manifolds: stable and unstable. The stable invariant manifold brings the small body closer to the periodic orbit, while the unstable one causes the small body to move away from the corresponding periodic orbit. The invariant manifold acts as a separatrix for the motion of small bodies. An object located inside the invariant manifold will transit to another region, while the object outside the invariant manifold will be bounced back to the original region [Gómez et al.(2001)]. Thus, the invariant manifold plays a major role in the transport and capture process of small bodies [Swenson et al.(2019)].

Table 1 shows the orbital parameter of 2020 CD_3 from observation data. In this study we have adopted the orbital parameters given by the Horizon System of JPL NASA website[5] which is based on JPL DE441 ephemerides [Park et al.(2021)]. For the case of 2020 CD_3, the data is available only from year ~ 2015. Hence, for our analysis, we considered 35 years of data starting from 2015 to 2050, with the step of one day. ICRF [Charlot et al.(2020)] is chosen as a reference frame. The barycenter of the Solar system was chosen as the origin and the data is given as position and velocity in cartesian coordinates.

We follow Method 1 of [Anderson & Lo(2016)] for transforming the asteroid trajectory into CRTBP. The concept of the transformation is briefly given as follows. The Cartesian orbital parameters (x, y, z, v_x, v_y, v_z) of the massless object are normalized and computed with respect to the primaries. These orbital parameters are converted to the rotational coordinates (X, Y, Z, V_X, V_Y, V_Z) with the primaries lying on the X-axis. The distance and time units are computed by fixing the condition of the primaries at the reference time, thus making the orbital parameters dimensionless. Here, the time and length units are defined from the instantaneous position and velocity of the primaries. The X-axis is based on the instantaneous vector from the Sun to the Earth, the Z-axis is aligned with the angular momentum vector of the motion of the Sun and Earth, and the Y-axis completes the right-handed system with the origin located at the barycenter of the two primaries.

Table 1: The orbital parameters of 2020 CD_3 at 2024-Oct-17. This data is taken from the JPL-NASA site (https://ssd.jpl.nasa.gov/sbdb.cgi). The meaning of each symbol is given by the following: eccentricity (e), semi-major axis (a), inclination (i), longitude of the ascending node (Ω), argument of periapsis (ω), and mean anomaly (M).

	Value	Uncertainty (1σ)
e	.01237592005052576	5.3939E-8
a (au)	1.029056248406796	2.5275E-8
i ($°$)	.6339854694301869	1.23E-7
Ω ($°$)	82.22841213520248	6.8997E-5
ω ($°$)	50.12530688163336	.00013469
M ($°$)	186.2546839004304	9.741E-5

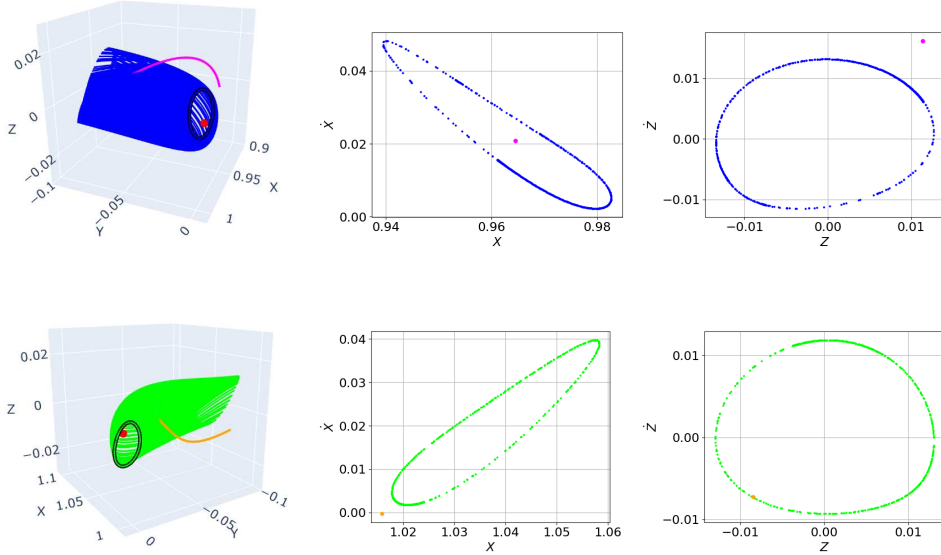
[5] https://ssd.jpl.nasa.gov/horizons/

2 Results

Fig. 8: 3D orbital dynamics of 2020 CD$_3$ (a and d) as well as the corresponding Poincaré sections of Halo's invariant manifolds in $\dot{X}, X$ (b and e) and $\dot{Z}, Z$ (c and f). Pre and post-capture orbits are shown in magenta and orange, respectively. Black line represents the Halo orbit. Blue and green lines represent the stable and unstable invariant manifold respectively. Lagrangian point is represented by a red dot. The trajectory is cut at $Y = -0.05$ for the Poincaré sections.

Fig. 2 shows the trajectory of the asteroid in 2D rotational coordinates of CRTBP. As shown in green line, we remarked that the object during its pre captured phase is always located in the left side of the zero velocity curve with the direction in counter-clockwise. The object enters the Earth's Hill region through L_1. During this period, it literally becomes Earth's TCO and stays such for a couple of years. The object then passes L_2 to orbit the Sun synchronously and the orientation of the movement becomes clockwise. Now, the orbit is located on the right side of the zero-velocity curve and will stay there.

As shown in Fig. 3a, the Jacobi constant in our case is not completely constant. There are some ripples in its time series due to a non perfect transformation from N-bodies to CRTBP. It should be noted that the CRTBP transformation has assumed several things. First, we limited the primaries only for the Sun and Earth-Moon barycentric. In the Hill region, the Moon has a non-negligible role in the asteroid trajectory. Meanwhile, other planets, notably Jupiter, have a role in perturbing the trajectory of the asteroid. The simplification of this trajectory might have produced certain defect. Moreover,

here we did not consider the system's eccentricity in the transformation. Since we consider the instantaneous primaries position and velocity as the length and time unit, the Earth's eccentricity will make these units vary, thus will affect the estimated Jacobian Constant.

The variation of Jacobi constant can be used as a rough tool for locating the time of entering the Hill zone of the Earth. As shown in the red region of Fig. 4, the ripples in Jacobi constant fluctuated between 2017 and 2020. This change of pattern can be interpreted as the captured event of the asteroid. This captured period matches the result of [de la Fuente Marcos & de la Fuente Marcos(2020)] where the asteroid was captured by the Earth between 2011 to 2018 and escaped from the Earth in $\sim$ 2020. Same energy level is needed for analysing the dynamics in CRTBP. Thus we need to fix the Jacobi constant. As the encounter with Earth severely changes the variation of Jacobi constant, we estimate this constant in two regions: before the encounter (C_{pre}) and after the encounter (C_{post}). We take the average value between $t_{pre} - 0.5$ years and $t_{pre} + 0.5$ years for C_{pre} while C_{post} is taken as the average value between $t_{post} - 0.5$ years and $t_{post} + 0.5$ years (see Figs. 3b and 3c). Hence we have $C_{pre} = 3.000172326819325$ and $C_{post} = 3.00030175227413$. Here t_{pre} and t_{post} mean the time of captured and escaped respectively. We calculated the Lyapunov and Halo periodic orbit with the nearest value possible of Jacobi constant to C_{pre} and C_{post}.

Here we treat the system in two- and three-dimensional perspectives. In the 2D case, the asteroid's orbit is projected onto the XY plane. Thus, the CRTBP transformation of the asteroid's orbital parameters must consider the value in the Z direction to be zero. We also consider the Lyapunov periodic orbit as well as its invariant manifold for the 2D case. Figs. 5a and 5b display the comparison between the asteroid's trajectory and the stable invariant manifold of the Lyapunov orbit in 2D case. Here the pink line represents the asteroid's trajectory during the pre-captured phase. The pre-captured trajectory follows the stable invariant manifold and ultimately ends up in the Lyapunov orbit L_1, serving as a gateway into the Hill region. For the post-captured event, the same pattern has also occurred (see Figs. 5d and 5e). After the asteroid escapes from the Hill region through L_2, the trajectory of the asteroid follows the unstable invariant manifold. Next, we investigate the Poincaré section by cutting the trajectory at $Y = -0.05$. As shown in Fig. 5c, the trajectory is inside the Poincaré section of the invariant manifold. It means that the asteroid's orbit is completely driven by the invariant manifold in pre-captured phase. This pattern also occurs for the post-captured phase. Here we recalculated the Poincaré section by using different cutoff. We found that the stable invariant manifold guides the asteroid's motion starting from $\sim$ 0.6 year before the capture event. In the post-capture phase, the motion is guided by the unstable invariant manifold for up to $\sim$ 0.8 year after the escape event.

Next, we examine the trajectory in 3D case ($Z \neq 0$). The Halo orbit and its invariant manifold are considered. Fig. 8 shows the comparison. Here we compared the pre- and post-captured trajectories with the invariant manifold of the northern Halo orbit. As shown in Fig. 7a, the trajectory of the asteroid in the pre-captured phase does not follow the invariant manifold. Meanwhile, we noted that the asteroid motion is inside the tube only when the position is near L_2 for the case of post-captured event (see Fig. 7d). The Poincaré surfaces are shown in Fig. 8. Here we analyze the Poincaré sections for X vs

$\dot{X}$ and Z vs $\dot{Z}$ by cutting the trajectory at $Y = -0.05$. During pre captured event, even if the trajectory is outside the invariant manifold in the space plot, the trajectory is inside the invariant manifold in the Poincaré surface plot for X vs $\dot{X}$. In contrast, the trajectory is inside the invariant manifold for post captured phase only in Z vs $\dot{Z}$.

Conclusions

In this paper, we have studied the orbital evolution of the asteroid 2020 CD$_3$ within the CRTBP framework. Here, we used the invariant manifold to study the corresponding trajectory in both two and three dimensions. In general, we found that the invariant manifold of the CRTBP matches the orbit of the asteroid. The pre-capture trajectory follows the stable invariant manifold and enters Hill region via L_1, while the post-capture one is entirely inside the unstable invariant manifold. The analysis of the Poincaré surfaces shows that the motion of the asteroid is completely controlled by the invariant manifold, notably ~ 0.6 years before the capture event (pre-capture) and ~ 0.8 years after the capture event (post-capture). This is not the case for halo orbit since the asteroid departs from its invariant manifold (either in position or velocity).

Acknowledgment

References

Anderson B. D. & Lo M. W., 2016, *In: Advances in the Astronautical Sciences Spaceflight Mechanics 2016, AAS 16-484: pp.1–19, 158. American Astron. Soc., California*

Anderson B. D. & Lo M. W., 2018, *In: Proceedings of Space Flight Mechanics Meeting 2018, pp.1087–1109. American Inst. for Aeronautics and Astronautics, Florida*

Charlot P., Jacobs C., Gordon D., Lambert S., De Witt A., Böhm J., Fey A., Heinkelmann R., Skurikhina E., Titov O., et al. 2020, *A & A, A159: p.1–28, 644*

de la Fuente Marcos C. & de la Fuente Marcos R., 2020, *MNRAS, p.1089–1094, 494*

de la Fuente Marcos C. & de la Fuente Marcos R., 2024, *Research Notes of the AAS, p.224, 8*

de la Fuente Marcos R., de León J., de la Fuente Marcos C., Licandro J., Serra-Ricart M., Cabrera-Lavers A., 2023, *A & A, L10:p.1–8, 670*

Fedorets G., Granvik M., Jones R. L., Jurić M., Jedicke R., 2020, *Icarus, 113517:p.1–9, 338*

Gómez G., Koon W. S., Lo M. W., Marsden J. E., Masdemont J., Ross S. D., 2001, *In: Advances in the Astronautical Sciences 2001, pp.3–22. American Astron. Soc., California*

Granvik M., Vaubaillon J., Jedicke R., 2012, *Icarus, p.262—277, 18*

Heppenheimer T., 1975, *Icarus, p.172—180, 24*

Horedt G., 1976, *AJ, p.675—680, 81*

Howell K., Marchand B., Lo M. W., 2001, *J. Astron. Sci., p.539—558, 49*

Koon W. S., Lo M. W., Marsden J. E., Ross S. D., 2001. *In: Dynamics of Natural and Artificial Celestial Bodies, pp.27–38. Springer, Dordrecht*

Kwiatkowski T., Kryszczyńska A., Polińska M., Buckley D., O'Donoghue D., Charles P., Crause L., Crawford S., Hashimoto Y., Kniazev A., et al., 2009, *A & A, p.967–974, 495*

Park R. S., Folkner W. M., Williams J. G., Boggs D. H., 2021, *AJ, 105:p1–15, 161*

Parker J. S. & Anderson R. L., 2014, *Low-Energy Lunar Trajectory Design, JPL DESCANTO Book Series, Volume 16, California*

Richardson D. L., 1980, *Celestial Mechanics, p.241—253, 22*
Rickman H. & Malmort A., 1981, *A & A, p.165--170, 102.*
Swenson T. E., Lo M. W., Woollands R. M., 2019, *MNRAS, p.2436--2447, 490*
Szebehely V., 1967, *Theory of Orbits, Academic Press, New York.*
Tancredi G., 1997, *Celest. Mech. Dyn. Astron., p.119--132, 69*